Published in final edited form as:
Biochemistry. 2011 November 22; 50(46): 10041–10051. doi:10.1021/bi2013454.

Allosteric Activation of Cytochrome P450 3A4 by α-Naphthoflavone: Branch Point Regulation Revealed by Isotope Dilution Analysis†

Caleb M. Woods, **Cristina Fernandez**, **Kent L. Kunze**, and **William M. Atkins***
Department of Medicinal Chemistry, University of Washington, Box 357610, Seattle, WA 98195-7610

Abstract

Cytochrome P450 3A4 is the dominant xenobiotic metabolizing CYP. Despite great interest in CYP enzymology, two *in vitro* aspects of CYP3A4 catalysis are still not well understood; namely, sequential metabolism and allosteric activation. We have therefore investigated such a system where both phenomena are present. Here we report that the sequential metabolism of Nile Red (NR) is increased by the heterotropic allosteric effector α-naphthoflavone (ANF). ANF increases the formation rates for NR metabolites M1 and M2, and also perturbs the metabolite ratio in favor of M2. Thus ANF has as an allosteric effect on a kinetic branch point. Coincubating deuterium labeled NR and unlabeled M1, we show that ANF increases the k_{cat}/k_{off} ~1.8 fold in favor of k_{cat} of M2 production. Steady-state metabolic experiments are analyzed using a kinetic model where enzyme and substrates are not in rapid equilibrium, and this distinction allows for the estimation of catalysis rates for the formation of both the primary (M1) and secondary (M2) products, as well as the partitioning of enzyme between these states. These results are compared with earlier spectroscopic investigations of NR and ANF cooperativity, and a mechanism of ANF heteroactivation is presented that involves effects on substrate off-rate and coupling efficiency.

Keywords

Sequential Metabolism; Allosterism; CYP3A4; Heteroactivation

Cytochrome P450 (CYP) enzymes catalyze the oxidation of xenobiotics and drugs, and contribute significantly to their pharmacokinetic properties. One isoform in particular, Cytochrome P450 3A4 (CYP3A4), is responsible for over 50% of oxidative drug metabolism due to its high expression levels in the liver and the gut as well as its extreme substrate promiscuity (1). CYP3A4 exhibits complex ‘atypical’ kinetics that complicate prediction of *in vivo* metabolism on the basis of *in vitro* kinetic parameters (2). These atypical kinetics reflect both homotropic and heterotropic allosteric effects. Despite the fact that α-Naphthoflavone (ANF; 7,8-benzoflavone) is a paradigmatic allosteric effector of numerous CYPs, the mechanism(s) by which it elicits these effects with CYP3A4 remain unexplained. For example, Schwab *et al.* (3) first reported that ANF acts as an effector molecule of testosterone 6β-hydroxylase and 17β-estradiol 2-hydroxylase metabolism in human liver microsomes, with similar results in rifampicin-treated and untreated rabbit liver

†This research was supported by National Institutes of Health Grant GM32165.

*To whom correspondence should be addressed. winky@uw.edu; telephone, (206) 685-0379; fax (206) 685-3252.

SUPPORTING INFORMATION AVAILABLE

Derivation of the equations used in the global analysis of Nile Red sequential metabolism with a discussion of the assumptions used in the analysis. This material is available free of charge via the Internet at http://pubs.acs.org.

microsomes. Shou *et al.* (4) reported ANF and phenanthrene metabolism mediated by CYP3A4 microsomes. Their results were interpreted in terms of multiple substrate binding, wherein both substrates affect each others' V_{Max}, but not each others' K_M, and thus have equal access to the active oxygen species. Although not applicable in all cases, this has subsequently become a common model for CYP allosterism (5).

Our group, along with others, has presented evidence that multiple ANF molecules bind to CYP3A4 and that the first binding event is largely 'silent' when observing changes in the ligand-dependent heme spin-state via optical difference spectroscopy and EPR (6). In a different approach, a fluorescently modified CYP3A4 was used to determine that testosterone (TST) binding does not compete with ANF, suggesting 'specific' binding sites for different effector molecules distal from the active site (7). This interpretation contrasts the previous model for ANF heterotropic allosterism based on the ability of both substrates to share the capacious, fluid active site (4, 8). Thus, the location of ANF at low and high occupancy remains unclear. While crystallographic evidence demonstrates the possibility that multiple molecules can simultaneously bind in the CYP3A4 active site (9), this has not been directly observed with ANF. Similarly, separate structural studies indicate a binding site for progesterone, which is distal from the heme (10), but the analogous situation for ANF has not been directly observed.

In addition to the uncertainty about the location of ANF molecules bound to CYP3A4 under varying conditions, the mechanism by which ANF causes heterotropic functional effects on CYP3A4 is not established. Non-Langmuir binding isotherms (e.g. sigmoidal) and non-Michaelis-Menten kinetics are often considered as evidence of multiple binding. However, multiple ligand binding in CYPs might occur without 'binding cooperativity' in the traditional sense, and could instead reflect differential affects on the heme spin state by the first versus subsequent ligands that bind (11, 12). Heterotropic activation, as observed with ANF and CYP3A4, could also arise from specific perturbations by the effector molecule on any of the rate determining steps in the P450 reaction cycle, regardless of its effect on substrate binding or substrate-induced spin-state changes. However, no studies have directly addressed the effect of ANF on the internal steps of the CYP reaction cycle. For example, the sequential oxidation of tertiary amines is a common route of drug metabolism, but the potential modulation by ANF or other allosteric effectors of branch points within sequential metabolism schemes has not been considered. Sequential, or processive metabolism catalyzed by CYPs, of both endogenous and exogenous compounds, has been reported and was the subject of a recent review (13).

In order to study allosteric effects on branch points within the CYP-catalyzed sequential metabolism of tertiary amines, here we use Nile Red (NR) as a fluorescent ligand and substrate for CYP3A4 and ANF as a heterotropic activator. The structure of NR, its metabolites, and ANF are shown in Scheme 1. Nile Red is sequentially metabolized via two N-deethylation reactions, allowing us to investigate an additional branch point between dissociation of the primary metabolite M1 (secondary amine) and oxidation to the secondary metabolite M2 (primary amine) (Scheme 2). In Scheme 2(a), the substrate A is NR in the current work, and B and C are M1 and M2, respectively. This is meant to show the general applicability of the experimental approach and the subsequently derived equations to any simple, two-step sequential metabolic pathway.

We have previously shown that NR is a fluorescent allosteric substrate of CYP3A4 (14) and that ANF and NR simultaneously bind to CYP3A4 (15). Furthermore, single molecule fluorescence experiments revealed a large ANF heterotropic effect resulting in a slower off-rate for NR from the ternary [CYP•ANF•NR] complex compared to [CYP•NR] (16). These, and other results, led us to further investigate NR sequential metabolism and

heteroactivation afforded by ANF. Here, we present evidence that supports the hypothesis that heterotropic allostery can result from effector modulation of specific branch points in the P450 cycle; specifically, the ratio of sequential, or processive Nile Red metabolism versus the dissociation of primary metabolite. Our results show definitively different kinetic behavior for effector-free and ANF-bound CYP3A4.

MATERIALS AND METHODS

Chemicals

All reagents were analytical grade and used without further purification unless otherwise specified. Solvents for LC-MS/MS were Optima LC-MS grade from Fisher. Solvents for flash chromatography and TLC were HPLC grade and from EMD chemicals (ethyl acetate) and OmniSolv (hexanes). All water used other than for LC-MS was deionized reverse osmosis Milli-Q quality from a Barnstead nanopureUV dispenser. Nile Red for kinetic and equilibrium experiments was high purity from Sigma Aldrich. Nile Red from TCI America was used for synthetic reactions. All other chemicals were from Sigma-Aldrich unless otherwise specified.

Protein Expression and Purification

Recombinant P450 3A4 was heterologously expressed in *E. coli* C41(DE3) cells. C41(DE3) cells made competent using the $CaCl_2$ method were transformed with pCWOri+ coding for ampicillin resistance and a CYP3A4 gene based on the Nf14 construct, an engineered 3A4 gene with an N-terminal truncation, and additionally modified with a C-terminal histidine tag (17, 18). Plasmid was isolated from transformed DH5α cells using the Qiagen maxiprep kit. A single colony of freshly transformed C41(DE3) cells was used to inoculate a 5 ml starter culture incubated overnight at 37°C in LB media supplemented to a final concentration of 50 μg/ml ampicillin. A 50 ml culture was inoculated from the starter culture and 5 ml was added to each 500 ml of TB media which was also supplemented with 50 μg/ml ampicillin and 0.5 ml of 1 M thiamine. After 4 hours at 37°C and shaking at 225 rpm, 0.5 ml of 1 M δ-ALA was added and cells were induced with 0.5 ml of 1M IPTG. Temperature and rpm were reduced to 27°C and 125 rpm respectively, and after 40 hours cells were harvested. Innoculum was centrifuged for 30 min at 4°C and 4500 rpm and the resulting pellets were frozen at −80°C. Aseptic technique was used throughout the cell culture procedure.

Cell pellets were thawed and resuspended in ice-cold resuspension buffer (100 mM KPi, 20% glycerol, 10 mM β-mercaptoethanol (BME), 2% Emulgen 911, pH 7.4) supplemented with protease inhibitor cocktail for His-tagged proteins (EDTA free), DNAse I, and 2 mg/ml lysozyme. The cell suspension was passed several times through a hand-held homogenizer and stirred at 4°C for 1 hour. The resulting suspension was centrifuged at 37000 rpm at 4°C for 60 min in a Ti45 rotor. The resulting pellet was discarded and the red supernatant was loaded directly onto a 30 ml Ni-NTA affinity column (Qiagen) equilibrated with wash buffer 1. After loading, the column was washed with 300 ml of wash 1 (50 mM KPi, 300 mM KCl, 40 mM imidazole, 20% glycerol, 2 mM BME, 0.2% Anapoe-$C_{10}E_9$, pH 7.4) followed by 300 ml of wash 2 (50 mM KPi, 300 mM KCl, 40 mM imidazole, 20% glycerol, 2 mM BME, 0.2% cholate, pH 7.4) and 1000 ml of wash 3 (50 mM KPi, 40 mM imidazole, 20% glycerol, 2 mM BME, 0.2% cholate, pH 7.4). Protein was eluted with elution buffer (50 mM KPi, 20% glycerol, 2 mM BME, 0.2% cholate, 400 mM imidazole) and dialyzed with 10,000 Da cutoff SnakeSkin pleated dialysis tubing (Thermo Scientific) against hydroxyapatite (HA) equilibration buffer; (10 mM KPi, 2 mM BME, 0.2% cholate, 20% glycerol) at 4°C. 50 μM TST was included in all buffers for Ni-NTA column chromatography but omitted from HA buffers. Dialyzed protein was loaded onto the HA column and then washed with 1000 ml

HA wash buffer, (25 mM KPi, 2 mM BME, 20% glycerol, pH 7.4). Protein was eluted with 400 mM KPi, 20% glycerol, pH 7.4, and dialyzed into storage buffer, 100 mM KPi, 20% glycerol, 1 mM EDTA, 500 μM TCEP, pH 7.4. The protein was diluted to ~20 μM and aliquoted and stored at −80°C for further use. Aliquots underwent no more than 5 freeze-thaw cycles each. Protein concentration was determined by 'dithionite difference spectra' (Fe^{+3}-H_2O vs. Fe^{+2}-CO) using an extinction coefficient of 99 mM^{-1} cm^{-1} (19, 20). This method is similar to that of Omura and Sato (Fe^{+2} vs. Fe^{+2}-CO) (21) but without the requisite anaerobic conditions in the reference cuvette. Protein was determined to be greater than 95% pure by reducing SDS-PAGE using a 10% acrylamide gel and staining with Coomassie brilliant blue.

Recombinant rat NADPH-Cytochrome P450 (Oxido)-Reductase (rCPR) was expressed as a fusion protein with the *omp*A signaling peptide in the pOR263 plasmid and purified as previously described by Shen, *et al* (22) with small modifications. Briefly, cultures were grown as for CYP3A4 expression except that LB was used and supplemented to 1 μg/ml riboflavin, 1 mM thiamine, and 100 μg/ml ampicillin. Expression was induced with 1 mM IPTG after 4 hours, and cultures were grown for a further 16 hours at 27° C and shaking at 125 rpm. Cells were pelleted by centrifugation at 4° C, briefly frozen at −80° C, and resuspended in cold lysis buffer (75 mM Tris pH 8, 0.25 M sucrose, 0.5 mM EDTA, 200 μM FMN, 0.02 mg/ml lysozyme, 0.5 μg/ml DNAseI, 50 μM DTT, with standard protease inhibitor cocktail purchased from Sigma-Aldrich (St Louis, MO), and stirred for one hour at 4° C. Lysate was passed through a French Pressure cell and centrifuged at 37,000 rpm for 45 min. The supernatant was discarded and the pellet resuspended with homogenization/wash buffer (50 mM Tris pH 7.7, 0.1 mM EDTA, 50 μM DTT, 10% glycerol, 0.15% Triton X-100) and passed through a hand-held homogenizer. Centrifugation at 37,000 rpm for 30 min afforded a yellowish-green supernatent which was loaded directly onto a 2′,5′-ADP Sepharose column equilibrated with wash buffer. The column was washed with 20 column volumes of wash buffer and eluted with a 0–6 mM NADP+ gradient in wash buffer with 0.1% Triton X-100. rCPR was buffer exchanged into storage buffer (100 mM KPi pH 7.5, 0.1 mM EDTA, 20% glycerol) via dialysis and size exclusion chromatography on a G-25 polyacrylamide sizing column equilibrated with storage buffer. rCPR was judged to be >95% pure by SDS-PAGE on an 8.25% reducing acrylamide gel stained with Comassie. rCPR concentration was determined by measuring the difference in absorbance between 456 and 550 nm of the purified protein in a solution of 0.01 mM $K_3Fe(CN)_6$ in 100 mM KPi using an extinction coefficient of 21.1 $mM^{-1}cm^{-1}$ (23).

Rat Cytochrome b_5 was a kind gift provided by Dr. Allan Rettie (University of Washington).

S_{50} determination using optical difference spectroscopy

Low to high spin state transitions upon binding of NR, metabolites, and ANF to CYP3A4 were preformed as previously described for NR (14, 15) using a dual-beam OLIS/Aminco DW2a spectrophotometer (OLIS, Bogart, GA). NR, metabolites, and ANF were titrated from DMSO stock solutions. DMSO concentration did not exceed 2% v/v.

Reconstituted System and Kinetic Assays

Determination of apparent kinetic constants K_M and V_{Max} using heterologously expressed human CYP3A4 followed the procedure of Shaw *et al*. (24) with some modifications as follows. Two 5x buffers, termed here 'dilution buffer' and 'reaction buffer,' contained the following: dilution buffer was 3 mM GSH, 50 mM Potassium HEPES; reaction buffer was 12 mM GSH, 200 mM Potassium HEPES. Both buffers were pH 7.4 at 37° C. To the dilution buffer was added a 100x solution of detergent and lipid containing 2 mg/ml L-α-dilauroyl-*sn*-glycerophosphocholine, L-α-dioleoyl-*sn*-glycero-3-phosphocholine, and L-α-

dilauroyl-*sn*-glycero-3-phosphoserine, at a 1:1:1 weight ratio per milliliter (Avanti Polar Lipids, Inc., Alabaster, AL) and 0.5 mg/ml CHAPS. This 100x stock solution was stored in screw-top eppendorf tubes, kept frozen until use, and was sonicated to clarity in 30s intervals alternating between bath sonicator at room temperature and wet ice. The bath sonicator was model 1510 from Branson operating at 40 kHz. To the lipid containing dilution buffer was then added CYP3A4, rCPR, and rCyt b5 in a 1:2:1 molar ratio. Final concentrations of enzyme in the 100 μl incubation were 30 nM CYP3A4, 60 nM rCPR, and 30 nM rCyt b5. The dilution buffer containing the enzymes was incubated for 10 min on ice with gentle mixing by hand. 20 μl of 5x reaction buffer was added to a 200 μl 96 well thin-walled PCR plate, to which was added 0.5 μl NR, M1, and/or ANF stock solutions in DMSO. All incubations were 1.5% DMSO. The PCR plate was then placed in a Rainin thermoshaker equipped with a PCR plate adapter and equilibrated at 37° C. Rotation was set at 1000 rpm. Control incubations contained the appropriate amount of DMSO. Water was added to the dilution buffer such that 68.5 μl of water + enzyme containing dilution buffer were added to each well, giving a volume of 90 μl. Wells were mixed by slow pipetting and incubated for 3 min at 37° C with shaking before addition of 10 μl of a freshly prepared 10x NADPH stock in H_2O, to give a final concentration of 1 mM, and total reaction volume of 100 μl. After 6 min the reactions were quenched into an equal volume (100 μl) of ice cold ACN in a 250 μl conical bottom 96 well plate containing carbamazepine as internal standard. This plate was then spun at 4000 rpm in a Sorvall Legend XTR centrifuge (Thermo Scientific) for 10 min and supernatant was transferred to a separate 96 well plate for LC-MS/MS analysis. Standard curves were created by subjecting known amounts of NR, M1, M2 and ANF to identical incubation conditions in the absence of NADPH. ANF metabolite was identified as the 5,6-epoxide based on daughter ion spectra (25) and concentration was estimated based on an ANF standard curve.

Isotope Dilution Experiments

Isotope Dilution experiments were performed following the same procedure for the NR kinetic assays with the exception that deuterated NR and unlabeled M1 were included in incubations. Deuterated NR and the deuterated metabolites produced by CYP3A4 were monitored in the d_2-(M+H+2) channel corresponding to the incorporation of two deuterium atoms relative to unlabeled NR. Several corrections were applied to the raw peak intensity as follows. The percentage of d_2-NR vs. total labeled NR was used to calculate the total amount of labeled NR and labeled metabolites. The amount of natural abundance ^{13}C causes a percentage of unlabeled M1 to appear in the d_2-M1 (M+H+2) channel, and this was corrected in both the d_2-M1 and d_2-M2 channels relative to unlabeled M1 and M2 intensities. The amount of unlabeled NR remaining in labeled NR (1.2%) was corrected in the M1 and M2 channels relative to d_2-M1 and d_2-M2 intensities. Standard curves and LC-MS/MS conditions were the same as those used for the kinetic experiments.

LC-MS/MS metabolite analysis

Metabolite identification and quantitation were preformed on an API 4000 triple quadrupole mass spectrometer in positive electrospray mode (MDS SCIEX, Concord, Ontario, Canada), coupled to two LC-10ADvp pumps with a SCL-10ADvp controller (Shimadzu, Columbia, MD) with a CTC PAL (Leap Technologies, Carrboro, NC) autosampler. The flow rate was 0.5 ml/min over a Zorbax-5μm SB-C_{18} 2.1 × 150 mm column (Agilent) with a gradient elution profile starting at 50% solvent A (H_2O with 0.1% FA) and 50% solvent B (ACN with 0.1% FA) and increasing to 95% B over 9 min, holding at 95% B for three min before returning to initial conditions. Retention times and MRM mass transitions are listed in Table 1. The desolvation temperature was 600° C, spray voltage 5.5 kV, and the declustering potential, collision energy, entrance and exit potentials optimized for each analyte.

Equations for fitting NR sequential Metabolism

Equations for the metabolism of a single substrate to sequential products can be derived from first principles based on both the Henri-Michaelis-Menten and Briggs-Haldane assumptions (26). The derivation based on the Briggs-Haldane assumptions is enumerated in the Supporting Information, and the equations used for data fitting are below where A, B, and C represent NR, M1, and M2 respectively.

$$\frac{d[B]}{dt}=\frac{V_{Max,B}\left(\frac{[A]}{K_{m,A}}\right)-V_{Max,C}\left(\frac{k_2}{k_3+k_4}\right)\left(\frac{[A]}{K_{m,A}}\right)-V_{Max,C}\left(\frac{[B]}{K_{m,B}}\right)}{1+\left(\frac{[A]}{K_{m,A}}\right)+\left(\frac{k_2}{k_3+k_4}\right)\left(\frac{[A]}{K_{m,A}}\right)+\left(\frac{[B]}{K_{m,B}}\right)+\left(\frac{k_4}{k_5}\right)\left(\frac{k_2}{k_3+k_4}\right)\left(\frac{[A]}{K_{m,A}}\right)+\left(\frac{k_4}{k_5}\right)\left(\frac{[B]}{K_{m,B}}\right)+\frac{[C]}{K_{d,C}}}$$

(Equation 1)

$$\frac{d[C]}{dt}=\frac{V_{Max,C}\left(\frac{k_2}{k_3+k_4}\right)\left(\frac{[A]}{K_{m,A}}\right)+V_{Max,C}\left(\frac{[B]}{K_{m,B}}\right)}{1+\left(\frac{[A]}{K_{m,A}}\right)+\left(\frac{k_2}{k_3+k_4}\right)\left(\frac{[A]}{K_{m,A}}\right)+\left(\frac{[B]}{K_{m,B}}\right)+\left(\frac{k_4}{k_5}\right)\left(\frac{k_2}{k_3+k_4}\right)\left(\frac{[A]}{K_{m,A}}\right)+\left(\frac{k_4}{k_5}\right)\left(\frac{[B]}{K_{m,B}}\right)+\frac{[C]}{K_{d,C}}}$$

(Equation 2)

The grouping of terms in the above equations has specific relevance to the sequential metabolism of NR as shown in Scheme 2(a). Specifically, the M2 formation can be sequential or dissociative, represented by the two terms in the numerator of Equation 2. The dissociative M2 formation rate (numerator, on the right) depends on the concentration of M1 in solution and the M1-CYP3A4 binding affinity. The sequential M2 formation rate (numerator, on the left) depends on the NR concentration in solution and the NR-CYP3A4 affinity, in addition to the M1 formation and M1 dissociation rates. In Equation 1, the numerator contains one term for M1 formation, but also contains the two terms for M1 depletion (ie. M2 formation). Several assumptions have been made to facilitate the use of these complex equations. First, it was assumed that there is no significant product inhibition, and so the term dependent on the $K_{d,C}$ can be ignored in the denominator. Also, the ratio of k_4/k_5 can thus be taken as zero, and two further terms can be ignored. Because the experimental conditions are such that NR is in excess and M1 concentration is low, combined with the fact that NR has a much tighter binding affinity than M1, we have ignored all dissociative enzyme-substrate complexes (i.e. those complexes that do not depend on NR concentration). Terms that include $K_{M,B}$ are thus ignored. These assumptions allow the use of the steady-state rate equations to analyze NR sequential metabolism under carefully controlled conditions, but care should be taken to recognize situations where these assumptions are invalid (e.g. when B or C are at high concentrations or if metabolites B and C have a tighter binding affinity than parent molecule A). As we will show, NR metabolism

is highly sequential and NR has tighter spectral binding affinity than its metabolites, and so we make these assumptions cautiously, but not without justification.

Isotope Dilution Equations

Analysis of the metabolism of labeled NR coincubated with unlabeled M1 is used to quantify sequential metabolism in CYP3A4 following a published procedure for the sequential metabolism of testosterone in CYP2C11 (27). In a similar fashion, we have used the amount of labeled and unlabeled NR metabolites to define two quantities A′ and B′ as follows:

$$A' = \frac{d_2M1}{d_2M1 + d_2M2} \quad \text{(Equation 3)}$$

and

$$B' = \frac{M2/M1}{1 - e^{(-M2/M1)}} \quad \text{(Equation 4)}$$

Deuterated and non-deuterated concentrations of metabolites were measured at the termination of six minte incubations using the same procedure as in the kinetic experiments. A′ and B′ are then used to calculate the ‘branching ratio’ k_{off}/k_{cat} (k_3/k_4 from Scheme 2a).

$$\frac{A' \times B'}{1 - A' \times B'} = \frac{k_{off}}{k_{cat}} \quad \text{(Equation 5)}$$

Please see ref. (27)for the full derivation of the equations listed above.

Synthesis of deuterated NR

Deuterium was incorporated into NR in 10% D_2SO_4, 20% anhydrous ACN, and 70% D_2O. The reaction was refluxed under a dry nitrogen atmosphere for 2.5 hours and reaction time points monitored by LC-MS at 30-minute intervals. LC-MS utilized a H_2O:ACN gradient (0.1% formic acid) and a 2.1 × 30 mm 3 μm AQUASIL C_{18} column (Thermo). Mass spectra were collected in positive ionization mode scanning 50–500 m/z. When d_0-NR was ~99% depleted, the reaction was quenched by cooling to 4° C and the addition of anhydrous K_2CO_3. Crude product was extracted extensively with cold ethyl acetate, washed with brine, dried over anhydrous $MgSO_4$ and filtered. EtOAc was concentrated with a rotovap and crude product was adsorbed onto silica. Product was purified using flash chromatography (gradient 1:0 – 1:1 hexanes/EtOAc). TLC on silica was monitored via uv detection: 2:1 hexanes-EtOAc, Rf 0.35. Peak integration for NR (m/z 319->275) and its deuterated products from LC-MS/MS chromatograms in MRM mode were performed under identical conditions as the isotope dilution experiments and indicated the following m/z distribution: 1.2% 319-d_0, 18.7% 320-d_1, 48.3% 321-d_2, 26.9% 322-d_3, 4.4% 323-d_4, and 0.5% 324-d_5.

Synthesis of M1

M1 was synthesized following the protocol of Olofson, *et al.* (28). Briefly, ten equivalents of 1-chloroethyl chloroformate and 1 equivalent of NR (TCI America) were refluxed in anhydrous toluene under a dry nitrogen atmosphere for 18 hours. After concentrating, the resulting crude chloroethyl carbamate ester was refluxed in 200 ml methanol with 1

equivalent of hydrochloric acid and monitored by TLC. The reaction was quenched by addition of solid $NaHCO_3$ and cold EtOAc was added. The combined organic fractions were washed with brine, dried over anhydrous $MgSO_4$, filtered, concentrated, and adsorbed onto silica for purification by flash column chromatography as described for deuterated NR (gradient 1:0 – 1:1 hexanes/EtOAc). Purity was assessed using HPLC as described above. TLC: 2:1 hexanes:EtOAc, Rf 0.21. ^{1}H-NMR (500 MHz CD_3CN) δ 8.6 (ddd, 1H, J = 8.0, 1.2, 0.6 Hz), 8.17 (ddd, 1H, J = 8.0, 1.5, 0.5 Hz), 7.76 (td, 1H, J = 7.5, 1.3 Hz), 7.67 (td, 1H, J = 7.5, 1.3 Hz), 7.54 (d, 1H, J = 9.0 Hz), 6.67 (dd, 1H, J = 9.0, 2.4 Hz), 6.46 (d, 1H, J = 2.5 Hz), 6.26 (s, 1H), 5.5 (s, 1H), 3.23 (qd, 2H, J = 7.5, 1.9 Hz), 1.23 (t, 3H, J = 7.5 Hz). Found m/z (M+H) 291.1134; within 0.3 ppm of theoretical monoisotopic $C_{18}H_{15}N_2O_2$.

Synthesis of M2

M2 was synthesized by modifying a reported synthesis for Nile Red from starting material Nile Blue (29). Cresyl Violet acetate salt (Acros) was refluxed in 0.5% H_2SO_4 with 20% ACN for 2 hours. The reaction was monitored by TLC and product was purified by flash column chromatography as described above. TLC: 2:1 hexanes:EtOAc, Rf 0.09. ^{1}H-NMR (500 Mhz CD_3CN) δ 8.56 (ddd, 1H, J = 8.0, 1.2, 0.4 Hz), 8.13 (ddd, 1H, J = 8.0, 1.3, 0.4 Hz), 7.74 (td, 1H, J = 7.5, 1.4 Hz), 7.65 (td, 1H, J = 7.5, 1.3 Hz), 7.51 (m, 1H), 6.65 (dd, 1H, J = 8.5, 2.4 Hz), 6.5 (d, 1H, J = 2.4 Hz), 6.22 (s, 1H), 5.14 (s, 2H). Found m/z (M+H) 263.0827; within 2.3 ppm of theoretical monoisotopic $C_{16}H_{11}N_2O_2$.

^{1}H-NMR spectroscopy of synthetic metabolites

^{1}H-NMR spectra were collected on a Varian 500 MHz Inova NMR spectrometer (Varian, Palo Alto, CA) using acetonitrile-d_3 or DMSO-d_6 as solvent. The saturation frequency was 499.735 MHz. Spectra were referenced to water. Proton assignments were assisted by ^{1}H-COSY and ^{1}H-ROESY homocorrelation 2D-NMR spectroscopy, which enabled the identification of the primary sights of deuterium incorporation in d-NR as the two most upfield aromatic protons.

High mass accuracy LC-MS/TOF

Synthetic NR metabolites and deuterated NR were analyzed on a Waters Synapt MS/TOF operated in positive electrospray mode coupled to an Agilant UPLC. Samples were introduced to the mass spectrometer via isocratic 80% ACN, 15% H_2O, 0.1% FA, with a 2.1 × 30 mm 3 μm AQUASIL C_{18} column (Thermo). Calibration used sodium formate scanning a mass range of 50–1000 m/z. Leucine-enkephalin (m/z 556.2771, 500 pg/μl) was constantly infused at a flow rate of 10 μl/min as internal standard.

RESULTS

Time Courses and Steady-State Kinetics of Nile Red Metablism

NR is metabolized by CYP3A4 to two predominant products; M1 (mono-des-ethyl-NR) and M2 (di-des-ethyl-NR), but the binding characteristics of M1 and M2 have not been determined previously. The net N-dealkylation of NR results from initial CYP3A4 mediated hydroxylation of the aliphatic methylene carbon on the diethylamino group to afford a carbinolamine (30, 31). This carbinolamine then spontaneously decomposes to an aldehyde and secondary amine (31). The secondary amine is subsequently oxidized in an analogous reaction, either prior to dissociation of M1 or after dissociation and rebinding of M1. NR sequential metabolism was monitored via LC-MS/MS. Chromatographic separation and unique mass transitions were used to unambiguously identify NR metabolites (Table 1) and concentration was determined from standard curves prepared from synthetic metabolites.

Figure 1 shows NR metabolite formation versus time. M2 production from the substrate NR shows a subtle but reproducible lag in formation. No lag in M2 production is apparent when M1 is the substrate nor is there a lag in M1 production from NR. The inclusion of ANF in the NR incubation increases the M2 formation rate and also decreases the lag as evidenced by the R^2 values for the linear regression of M2 concentration versus time curves in Figure 1. These data suggest intuitively that some dissociative metabolism occurs during the conversion of NR to M2, and that ANF alters the internal reaction dynamics or branch points. More striking is the relative rate of formation of M2 with saturating NR versus saturating M1. M2 is formed slightly faster from NR than M1 in the absence of ANF, and significantly faster in its presence. This is an intriguing indication that NR activates its own metabolism, and does so to a greater extent than M1 activates its own metabolism. Because the amount of M2 metabolite formed with saturating NR is comparable to the amount of M2 formed with saturating M1, and because significant amounts of M1 are also produced when NR is saturating, we surmise that NR can act as a homotropic activator. In effect, more M2 is made from NR than from saturating M1, the upstream metabolite, and this demands that NR activates its own metabolism to M2. Previous spectroscopic evidence has established the multiple binding behavior of NR with and without ANF (14, 15). The ability of ANF, NR, and M1 to act as an allosteric effector would thus be rank ordered as ANF>NR>M1.

Figure 3 shows the steady-state kinetics of NR turnover. Total metabolite formation was fit to the M-M equation to give K_M values for NR metabolism at 0 and 12 μM ANF. These K_M's were used to parameterize the B-H fitting equations. M1 and M2 formation are saturable by NR, and in fact the apparent K_M for M1 and M2, with NR as substrate, are not experimentally distinguishable. Because both M1 and M2 formation depend on NR concentration, it is likely that M2 production is highly sequential. Fitting the sequential metabolism to the B-H equations provides estimates of the individual catalytic rate constants (V_{Max}) based on enzyme partitioning to the NR and M1 bound species. Results from Figure 3 are summarized in Table 2 and Scheme 2b.

Spin State Perturbation

The equilibrium affinity of substrates and metabolites is a critical determinant of the kinetic behavior of sequential metabolism schemes. If the metabolites bind with sufficiently high affinity, a greater fraction of downstream products will arise from nondissociative metabolism. Conversely, if the metabolites bind with low affinity compared to substrate, this will increase the tendency for dissociative metabolism. Binding affinities of NR and ANF to CYP3A4 were determined via UV/Vis titrations as done previously, but results are shown here for comparison with the NR metabolite spectra (6, 14). Like ANF and NR, both the metabolites M1 and M2 yield type I difference spectra indicative of a perturbation to high-spin heme from the low-spin resting state. All ligands show pronounced sigmoidal behavior in the binding isotherms (Figure 2). Recovered S_{50}'s from fits to the Hill equation are 7.3, 68, and 58 μM for NR, M1, and M2 respectively. The NR metabolites have significantly lower affinity for CYP3A4 as judged by the spin-state titrations. One interpretation of the sigmoidal spin-state changes is that multiple molecules bind with the first having little or no effect on the spin state while the second, or subsequent, binding event causes a perturbation to high spin. This does not necessarily indicate that the binding events are cooperative in the traditional definition, as pointed out previously (11, 12). When compared to the turnover kinetics, the spin state results are quite striking, as NR turnover can be fit to a hyperbola with no indication of sigmoidicity (Figure 3), unlike ANF turnover, which is sigmoidal at low concentrations, prior to the apparent substrate inhibition (data not shown, results below) (32). An important result of these experiments is that M1 and M2 have significantly lower affinity for CYP3A4 than does NR.

ANF as a substrate

In order to understand the allosteric effects of ANF on NR sequential metabolism, it is necessary to account for possible ANF metabolism in co-incubations that include ANF with either NR or M1. Therefore, we determined the apparent kinetic parameters for ANF turnover in our experimental conditions. The only ANF metabolite detected was the 5,6-oxide as indicated by the fragmentation pattern and mass transition m/z 289->131 as presented by Shou *et al.* (25). The velocity vs. [ANF] plots are complex, with sigmoidal shape at low concentration and apparent substrate inhibition at high concentrations. These results are consistent with those of Sligar *et al.* (32) in that ANF binds to CYP3A4 with a stoichiometry of up to 3 ANF molecules per CY3A4. Our proposed stoichiometry is based on the pronounced sigmoidicity at low [ANF] and substrate inhibition at high [ANF]. This suggests the third ANF binding site causes some inhibition. The approximate S_{50} for the ANF turnover in the lower concentration range is 10 μM, which is significantly above the apparent K_M for NR (2–3 μM). The estimated V_{Max} is 0.02 nmol/min/nmol CYP for epoxidation of ANF obtained from the peak rate in the complex velocity vs. [ANF] plot (not shown). This rate is slower than some previously published results (33, 34) based on HPLC to estimate ANF metabolite, and which used a different CYP:CPR:b5 ratio. In addition modest changes in purification procedures or buffer components could contribute to the variable rates. The important result of this direct comparison is that ANF is metabolized much less efficiently than NR, and under the conditions used here it does not compete with NR for metabolism. Therefore, in some of the subsequent experiments, the concentration of ANF is assumed to not change. In addition, the results indicate that the allosteric effects of ANF, described below, occur at concentrations that do not afford metabolites or significant heme spin-state changes.

ANF acts as an effector of NR metabolite formation

ANF increases the amount of M2 that is produced in the NR incubations, while having negligible effect on the amount of M1 produced (Figure 3). An important aspect of sequential metabolism of NR is that all M1 formed is not released into the medium, as some is retained on the enzyme and subsequently oxidized. That is to say, although apparent M1 formation rates are similar with and without ANF, the actual NR depletion rate, and thus M1 formation rate, must be increased in the presence of ANF even though the largest measurable experimental outcome is the dramatic increase in M2 formation. In other words, the total amount of NR metabolism increases in the presence of ANF, with the largest effect being on M2 production. ANF exerts its effects mainly on V_{Max}, with the experimentally determined K_M values for NR total metabolite production increasing slightly as ANF concentration is increased. ANF therefore does not increase CYP3A4 affinity for NR, but acts to increase the V_{Max} term in the velocity equations. Steady-state analysis of NR sequential metabolism indicates that ANF increases the velocity of both M1 and M2 formation. The steady-state model used here, however, does not include uncoupling, and the V_{Max} terms are thus aggregate kinetic constants that include multiple steps in the P450 catalytic cycle.

Isotope Dilution Analysis

Isotope dilution analysis provides a quantitative measure of the relative flux of an intermediate in the reaction cycle, such as [CYP•M1], forward to yield the secondary product [CYP•M2], compared to the dissociation of the [CYP•M1] complex (27). The measured ratio of forward flux to dissociation is independent of the absolute rates of these processes. In Scheme 2, this represents the bifurcation of the [CYP•M1] complex to either of two fates, dissociation to free enzyme and M1, or further metabolism to the [CYP•M2] complex. The relative magnitude of the catalytic rate constant k_4 versus the off-rate for the [CYP•M1] complex k_3 defines the amount of sequential metabolism and will be referred to

as a branching ratio. Some P450s, such as CYP19A1 (aromatase), have been shown to be highly sequential enzymes, in that metabolic intermediates (19-OH androstenedione and 19-oxo androstenedione) rarely dissociate and substrate undergoes multiple rounds of P450 catalysis before the final product, estrone, is ultimately released into solution (13). A separate study using rat CYP2C11 indicated that testosterone sequential metabolism to 16α-hydroxyandrostenedione was predominantly dissociative (27). It does not appear possible to predict *a priori* the level of sequential metabolism for a given enzyme-substrate pair, and the determinants for highly sequential metabolism in P450s are, as of yet, undefined. It is likely that some enzymes evolved this capability, while others, such as CYP3A4, display this kinetic behavior in the apparent absence of a specific evolved function or particular metabolic advantage.

Incubations of deuterium labeled NR and unlabeled M1 were performed using the same procedures as for the experiments with unlabeled NR. Yields of labeled and unlabeled NR metabolites were quantified using LC-MS/MS and analyzed according to the methods outlined by Sugiyama *et al.*(27). Results from the kinetic experiments suggested that ANF acts by increasing the amount of sequential metabolism, and this was corroborated by the isotope dilution results. In the absence of ANF the branching ratio, k_{off}/k_{cat}, is 4.38 ± 0.62, and represents a ratio where the off-rate of the [CYP•M1] complex is 4.38 times that of the catalysis rate to form the [CYP•M2] complex. In the presence of ANF the ratio decrease to 2.42 ± 0.31 which indicates that either the off-rate is attenuated, the catalysis rate augmented, or a combination of the two.

Simulations of branch point modulation

Simulations of NR sequential metabolism were carried out using COPASI software with enzyme concentration set at 30 nM. Individual rate constants were manipulated as shown in Figure 5. The metabolite ratio can be manipulated by changing the off-rate of M1. Importantly, however, the K_d need not change for the complex [M1•CYP3A4] in order for this off-rate effect to manifest as a change in metabolite ratio. This effect would not be observed under conditions where substrates and enzyme were in rapid equilibrium as postulated in the derivation of the Micaelis-Menten equation. We show two simulations where only the on-rate and off-rates of M1 are changed (k_{-3} and k_3). Because the off-rate and the catalysis rate branch from a single species, changing the off-rate relative to the catalysis rate, even when the enzyme-substrate affinity is not changed and the catalysis rate k_4 is unchanged, still results in a large effect in metabolite ratio.

DISCUSSION

These studies are aimed at further understanding sequential metabolism and heterotropic allosteric activation, which are two well-appreciated aspects of CYP3A4 enzymology. Although sequential metabolism and allosteric effects are well-appreciated, the two aspects have not been considered in combination. Many drug molecules containing tertiary amines are dealkylated, and importantly this process can occur iteratively, sometimes with the generation of tight binding inhibitory complexes (35). Circulating levels of these drug metabolites are of increasing interest to CYP inhibition and drug-drug interactions (36). Predicting metabolite concentrations of sequential systems will depend on increased mechanistic understanding of CYP catalyzed sequential metabolism in general. Models that probe allosteric effects in sequential metabolism are likely to be valuable.

The model we develop here highlights the need for non-Michaelis-Menten analyses with sequential allosteric systems. Before we introduce our kinetic model, some qualitative analysis of NR sequential metabolism with emphasis on observed phenomenological trends is valuable. In the rapid equilibrium (M-M) assumption the product off-rate is assumed to be

fast relative to the catalytic rate, but the sequential nature of NR metabolism suggests that the NR sequential system is not in rapid equilibrium. If the M1 off-rate is very fast relative to M2 formation all M2 will be formed dissociatively (i.e. nonsequentially). Conversely, if M2 formation was predominantly sequential, with very little M1 release followed by rebinding to the enzyme to be metabolized to M2, then M2 formation would depend on NR concentration and M2 formation plotted versus NR concentration would display saturable hyperbolic behavior. We observe, in Figure 3, that M2 formation is indeed saturable by NR and is reasonably described by a hyperbola, and the K_M for M2 production is not statistically distinguishable from the K_M for M1 production. This indicates that M2 production is dependent on NR concentration and likely proceeds largely from the [CYP•NR] complex, and is 'significantly' sequential. The presence of the intermediate primary metabolite (M1) in solution indicates that the M1 off-rate and M2 catalysis rates are similar, and is important evidence that the process is not completely sequential. If none or very little M1 was detected, one might conclude that the M2 catalysis rate is much faster than the M1 off-rate, but this is not found to be the case. These qualitative observations indicate that M2 production is at least partially sequential, and that the M2 catalysis rate and M1 off-rate are similar.

To enable a more quantitative assessment of NR sequential metabolism, steady-state rate equations were derived based on the microscopic rate constants as shown in Scheme 2a. These equations enable the approximation of the catalytic rates because the B-H equations explicitly include the sequential nature of NR metabolism and the competition of substrate and primary metabolite for free enzyme. Because most terms are shared between equations, an added benefit of this analysis is the possibility of analyzing M1 and M2 formation rates globally, linking all shared terms. One disadvantage of this approach is that the complexity of the equations makes the explicit treatment of allosterism intractable. Instead, we have performed experiments at several ANF concentrations and examined the trends in affinity and velocity parameters phenomenologically. A full ANF concentration analysis would be attractive, but because of the inability of rapid equilibrium assumptions to describe NR sequential metabolism we instead interpret the velocity and branching ratio data as a representation of concentration weighted averages of homotropic species [NR•E•S] and heterotropic species [ANF•E•S] (S is NR or M1) without specific information on binding stoichiometry. Still, the experiments are highly informative regarding the ANF effects, particularly when considering the cases of minimum and maximum ANF effects, which report on the homotropic and heterotropic species.

ANF causes an increase in total metabolite formation (green traces, Figure 3) from NR, but has a larger effect on the relative amount of M2 vs. M1 produced (orange and pink traces, Figure 3). This occurs at concentrations of ANF that do not contribute significant competitive inhibition to NR turnover. The ANF K_s has been determined to be 10.7 μM when fit to the Hill equation (data not shown), but the amount of ANF product 5,6-oxide produced at that concentration is ~1000 fold less than total NR metabolite formation. The ANF metabolism data are intriguing to compare to the ANF stimulation of NR metabolism. These data suggest that while the first ANF binding event does not contribute to ANF turnover, it significantly augments NR metabolism. This observation is interesting when compared to earlier fluorescence experiments (15), which were interpreted as evidence for ANF binding to a peripheral binding site, where ANF and NR compete for this 'allosteric' site. Thus, the two results are consistent with one another in as much as they suggest that a high-affinity binding site for ANF exists distal from the immediate heme environment, and this binding site modulates NR metabolism.

Previous experiments support a model in which NR binds to CYP3A4 at multiple sites, and ANF also binds to CYP3A4 and competes with NR for one, but not both, binding sites at

low ANF concentrations (15). Subsequent single molecule fluorescence experiments showed that the NR off-rate was attenuated in the presence of ANF (16). Although NR sequential metabolism and ANF heteroactivation give complex kinetics, incorporating previous biophysical experiments with kinetic data allows for the generation of a mechanistic model of allosteric activation in CYP3A4. Analysis of NR sequential metabolism suggests that ANF acts by modulating the branching at sensitive points in the P450 cycle. The data in Table 2 are estimated from the global fitting parameters derived from data in Figure 3. Scheme 2b summarizes the global fitting parameters in the context of the NR sequential kinetic model. Because of the complexity of the sequential system, with the additional homotropic and heterotropic allosterism, we sought an experimental technique that used some of the inherent complexities of NR sequential metabolism to our advantage.

Isotope dilution, analogous to traditional pulse-chase experiments, has been used to study CYP mediated sequential metabolism (27). Rather than pulse with isotopically labeled substrate and chase with 'cold' substrate, the experimental design calls for coincubation of isotopically labeled substrate (d-NR) and non-labeled primary metabolite (M1). The amounts of labeled and unlabeled secondary metabolite (M2) can then be used to approximate the amount of sequential (d-M2) vs. dissociative secondary metabolite (M2). The unlabeled M1 acts as a competitive inhibitor of released labeled d-M1 from the enzyme, and corrects for 'dissociatively' produced d-M2. We have carried out isotope dilution experiments on NR sequential metabolism with deuterated NR, prepared according to the Materials and Methods. The specific output of these experiments, termed here the 'branching ratio' (k_{cat}/k_{off}), refers to the microscopic rate constants k_4 and k_3 in Scheme 2a. We offer two interpretations of this ratio. The first interpretation disregards coupling effects. In the absence of uncoupling, which would present an additional branching pathway from the active [E•M1] complex, the ratios of labeled and unlabeled NR metabolites simplify to the k_{off}/k_{cat} branching ratio. Because we can approximate k_{cat} (k_4) from kinetic experiments we can estimate the k_{off} term, and as shown in Figure 4 ANF causes a large shift in this ratio. The concentration dependence of this shift is also important to the model, because it shows no sigmoidal behavior. However this ratio does decrease at high ANF concentrations. The simple interpretation of these data agrees with the original single molecule fluorescence work (16) is that ANF appears to increase the residence time of substrate, or metabolite, in the CYP3A4 active site. The observation of ANF effects on NR binding in CYP3A4 nanodiscs are consistent with the isotope dilution results in turnover system utilized here, which includes not only lipid and detergent, but also the redox partner proteins CPR and CYT b_5.

The mass spectral isotope dilution data unambiguously demonstrate that the branching ratio k_4/k_3 increases in the presence of ANF. This could be due to an increase in apparent k_4, a decrease in k_3, or both. Therefore, simulations of NR sequential metabolism were carried out to distinguish possible mechanisms for ANF heteroactivation. The results of the simulations and the experimental results are only consistent with the later. The best fit of the simulated kinetic scheme to the experimental data (Scheme 2) demonstrates that k_2 and k_4 values for both M1 formation and M2 formation increase to a nearly identical extent when ANF is added. There is no differential affect of ANF on k_2 vs. k_4, which increase by 2.1-fold and 2.3-fold respectively. However, with the constraint that k_2 and k_4 increase by nearly equal amounts, in order to observe the inversion of the product ratio, which favors M1 in the absence of ANF, to favor M2 in the presence of ANF, the off-rate for M1 must decrease in its presence, as indicated by the recovered parameters form the simulations, wherein the off-rate k_3 decreases by 1.8-fold. In other words, given that the recovered k_2 and k_4 parameters increase for both M1 and M2 production to the same extent but the product ratio changes, it is clear that an internal branching ratio must change, as proven by the isotope dilution data. Thus the simulations that reproduce the observed experimental kinetic

behavior is consistent with the isotope dilution results. In addition, the results (Table 2) indicate that there is an increase in the relative fraction of the enzyme as [CYP•M1] vs. [CYP•NR] in the presence of ANF. This occurs despite the fact that both k_2 and k_4 rate constants increase to the same extent. The relative increase in [CYP•M1] with the nearly identical increase in k_2 and k_4 demands that k_3 decreases. The molecular basis for the cause of an increase in k_2 and k_4 is not addressed by the current studies. One possibility is that the actual chemical step for hydrogen atom abstraction by the perferryl iron-oxo intermediate is faster. Alternatively, a faster k_2 or k_4 could be obtained if uncoupling to reduced oxygen species was slower in the presence of ANF. This would effectively increase the steady state concentrations of [CYP•M1] and [CYP•NR] and increase the rate of M2 or M1 formation, respectively. Together the isotope dilution results and the best fit of the kinetic data to the model suggest that there is either an increase in coupling or an increase in the rate of hydrogen abstraction and rebound, *and* a decrease in off-rate for M1. While this conclusion is consistent with our previously published data concerning the effects of ANF on the off-rate of NR, it raises the additional hypothesis that uncoupling is decreased in the presence of ANF. Future work will focus on the quantitative effects on these isolated parameters. We speculate that uncoupling is decreased by ANF.

Regardless of the complexity of the sequential metabolic scheme, the data presented herein unambiguously demonstrate branch-point modulation by the allosteric effector where substrate off-rates are attenuated (or k_{cat} is increased) and apparent kcat for M1 increases. This does not necessarily require an ANF-induced change in substrate affinity as shown by kinetic simulation. Although we cannot infer the location of ANF binding, it is clear that ANF, at low concentrations, binds to CYP3A4 and activates, rather than inhibits NR metabolism. This activation causes small changes in the branching ratios to different products from a crucial intermediate during the P450 cycle, the oxygen associated [E•S] complex, and this small change in branching ratios causes rather significant changes in metabolite production.

Supplementary Material

Refer to Web version on PubMed Central for supplementary material.

Acknowledgments

C.M.W. acknowledges support from the ACS Division of Medicinal Chemistry and Pfizer Inc., as well as the ARCS foundation, Seattle chapter.

Abbreviations

ACN	acetonitrile
δ-ALA	δ-aminolevulinic acid
ANF	α-Naphthoflavone (7,8-benzoflavone)
B-H	Briggs-Haldane
BME	β-mercaptoethanol
CHAPS	3-[(3-Cholamidopropyl)dimethylammonio]-1-propanesulfonate
CYP3A4	Cytochrome P450 3A4
Da	Dalton
d-NR	deuterated Nile Red

DMSO	dimethyl sulfoxide
EDTA	ethelenediaminetetraacetic acid
EPR	electron paramagnetic resonance
FA	formic acid
FMN	flavin mononucleotide
GSH	glutathione
HA	hydroxyapatite
IPTG	isopropyl β-D-1-thiopyranoside
KPi	potassium phosphate
LB	Luria-Bertani medium
M1	mono-des-ethyl-Nile Red
M2	di-des-ethyl-Nile Red
M-M	Michaelis-Menten
m/z	mass to charge ratio
NR	Nile Red (7-diethylamino-3,4-benzophenoxizine-2-one)
PCR	polymerase chain reaction
ppm	parts per million
rCPR	rat Cytochrome P450 reductase
rCYT b_5	rat Cytochrome b5
Rf	retention factor
rpm	rotations per minute
SDS-PAGE	sodium dodecly-sulfate polyacrylamide gel electrophoresis
TB	terrific broth
TCEP	Tris(2-carboxyethyl)phosphine
TLC	thin layer chromatography
TOF	time-of-flight
TST	testosterone

References

1. Guengerich FP. Cytochrome P450 and chemical toxicology. Chem Res Toxicol. 2008; 21:70–83. [PubMed: 18052394]
2. Atkins WM. Non-Michaelis-Menten kinetics in cytochrome P450-catalyzed reactions. Annu Rev Pharmacol Toxicol. 2005; 45:291–310. [PubMed: 15832445]
3. Schwab GE, Raucy JL, Johnson EF. Modulation of rabbit and human hepatic cytochrome P-450-catalyzed steroid hydroxylations by alpha-naphthoflavone. Mol Pharmacol. 1988; 33:493–499. [PubMed: 3367901]
4. Shou M, Grogan J, Mancewicz JA, Krausz KW, Gonzalez FJ, Gelboin HV, Korzekwa KR. Activation of CYP3A4: evidence for the simultaneous binding of two substrates in a cytochrome p450 active site. Biochemistry. 1994; 33:6450–6455. [PubMed: 8204577]

5. Davydov DR, Halpert JR. Allosteric P450 mechanisms: multiple binding sites, multiple conformers or both? Expert Opin Drug Metab Toxicol. 2008; 4:1523–1535. [PubMed: 19040328]
6. Roberts AG, Atkins WM. Energetics of heterotropic cooperativity between alpha-naphthoflavone and testosterone binding to CYP3A4. Arch Biochem Biophys. 2007; 463:89–101. [PubMed: 17459328]
7. Tsalkova TN, Davydova NY, Halpert JR, Davydov DR. Mechanism of interactions of alpha-naphthoflavone with cytochrome P450 3A4 explored with an engineered enzyme bearing a fluorescent probe. Biochemistry. 2007; 46:106–119. [PubMed: 17198380]
8. Korzekwa KR, Krishnamachary N, Shou M, Ogai A, Parise RA, Rettie AE, Gonzalez FJ, Tracy TS. Evaluation of atypical cytochrome P450 kinetics with two-substrate models: evidence that multiple substrates can simultaneously bind to cytochrome P450 active sites. Biochemistry. 1998; 37:4137–4147. [PubMed: 9521735]
9. Ekroos M, Sjögren T. Structural basis for ligand promiscuity in cytochrome P450 3A4. Proc Natl Acad Sci USA. 2006; 103:13682–13687. [PubMed: 16954191]
10. Williams PA, Cosme J, Vinkovic DM, Ward A, Angove HC, Day PJ, Vonrhein C, Tickle IJ, Jhoti H. Crystal structures of human cytochrome P450 3A4 bound to metyrapone and progesterone. Science. 2004; 305:683–686. [PubMed: 15256616]
11. Denisov IG, Frank DJ, Sligar SG. Cooperative properties of cytochromes P450. Pharmacol Ther. 2009; 124:151–167. [PubMed: 19555717]
12. Roberts AG, Campbell AP, Atkins WM. The thermodynamic landscape of testosterone binding to cytochrome P450 3A4: ligand binding and spin state equilibria. Biochemistry. 2005; 44:1353–1366. [PubMed: 15667229]
13. Guengerich F, Sohl C, Chowdhury G. Multi-step oxidations catalyzed by cytochrome P450 enzymes: Processive vs. distributive kinetics and the issue of carbonyl oxidation in chemical mechanisms. Arch Biochem Biophys. 2011; 507:126–134. [PubMed: 20804723]
14. Lampe JN, Fernandez C, Nath A, Atkins WM. Nile Red is a fluorescent allosteric substrate of cytochrome P450 3A4. Biochemistry. 2008; 47:509–516. [PubMed: 18092806]
15. Nath A, Fernández C, Lampe JN, Atkins WM. Spectral resolution of a second binding site for Nile Red on cytochrome P4503A4. Arch Biochem Biophys. 2008; 474:198–204. [PubMed: 18395506]
16. Nath A, Koo PK, Rhoades E, Atkins WM. Allosteric effects on substrate dissociation from cytochrome P450 3A4 in nanodiscs observed by ensemble and single-molecule fluorescence spectroscopy. J Am Chem Soc. 2008; 130:15746–15747. [PubMed: 18980315]
17. Gillam EM, Baba T, Kim BR, Ohmori S, Guengerich FP. Expression of modified human cytochrome P450 3A4 in Escherichia coli and purification and reconstitution of the enzyme. Arch Biochem Biophys. 1993; 305:123–131. [PubMed: 8342945]
18. Domanski TL, Liu J, Harlow GR, Halpert JR. Analysis of four residues within substrate recognition site 4 of human cytochrome P450 3A4: role in steroid hydroxylase activity and alpha-naphthoflavone stimulation. Arch Biochem Biophys. 1998; 350:223–232. [PubMed: 9473295]
19. Matsubara T, Koike M, Touchi A, Tochino Y, Sugeno K. Quantitative determination of cytochrome P-450 in rat liver homogenate. Anal Biochem. 1976; 75:596–603. [PubMed: 984414]
20. Rutten AA, Falke HE, Catsburg JF, Topp R, Blaauboer BJ, van Holsteijn I, Doorn L, van Leeuwen FX. Interlaboratory comparison of total cytochrome P-450 and protein determinations in rat liver microsomes. Reinvestigation of assay conditions. Arch Toxicol. 1987; 61:27–33. [PubMed: 3439870]
21. Omura T, Sato R. The carbon monoxide-binding pigment of liver microsomes. I Evidence for its hemoprotein nature. J Biol Chem. 1964; 239:2370–2378. [PubMed: 14209971]
22. Shen AL, Porter TD, Wilson TE, Kasper CB. Structural analysis of the FMN binding domain of NADPH-cytochrome P-450 oxidoreductase by site-directed mutagenesis. J Biol Chem. 1989; 264:7584–7589. [PubMed: 2708380]
23. French JS, Coon MJ. Properties of NADPH-cytochrome P-450 reductase purified from rabbit liver microsomes. Arch Biochem Biophys. 1979; 195:565–577. [PubMed: 112928]
24. Shaw PM, Hosea NA, Thompson DV, Lenius JM, Guengerich FP. Reconstitution premixes for assays using purified recombinant human cytochrome P450, NADPH-cytochrome P450 reductase, and cytochrome b5. Arch Biochem Biophys. 1997; 348:107–115. [PubMed: 9390180]

25. Shou M, Dai R, Cui D, Korzekwa KR, Baillie TA, Rushmore TH. A kinetic model for the metabolic interaction of two substrates at the active site of cytochrome P450 3A4. J Biol Chem. 2001; 276:2256–2262. [PubMed: 11054425]
26. Segel, IH. Enzyme Kinetics: Behavior and Analysis of Rapid Equilibrium and Steady-State Enzyme Systems. John Wiley and Sons, Inc; New York: 1993.
27. Sugiyama K, Nagata K, Gillette JR, Darbyshire JF. Theoretical kinetics of sequential metabolism in vitro. Study of the formation of 16 alpha-hydroxyandrostenedione from testosterone by purified rat P450 2C11. Drug Metab Dispos. 1994; 22:584–591. [PubMed: 7956734]
28. Olofson RA, Martz JT, Senet JP, Piteau M, Malfroot T. A new reagent for the selective, high-yield N-dealkylation of tertiary amines: improved syntheses of naltrexone and nalbuphine. J Org Chem. 1984; 49:2081–2082.
29. Greenspan P, Fowler SD. Spectrofluorometric studies of the lipid probe, nile red. J Lipid Res. 1985; 26:781–789. [PubMed: 4031658]
30. Wang Y, Kumar D, Yang C, Han K, Shaik S. Theoretical study of N-demethylation of substituted N,N-dimethylanilines by cytochrome P450: the mechanistic significance of kinetic isotope effect profiles. J Phys Chem B. 2007; 111:7700–7710. [PubMed: 17559261]
31. Upthagrove AL, Nelson WL. Carbinolamines, imines, and oxazolidines from fluorinated propranolol analogs. (19)F NMR and mass spectral characterization and evidence for formation as intermediates in cytochrome P450-catalyzed N-dealkylation. Drug Metab Dispos. 2001; 29:1114–1122. [PubMed: 11454730]
32. Frank DJ, Denisov IG, Sligar SG. Analysis of heterotropic cooperativity in cytochrome P450 3A4 using alpha-naphthoflavone and testosterone. J Biol Chem. 2011; 286:5540–5545. [PubMed: 21177853]
33. Ueng YF, Kuwabara T, Chun YJ, Guengerich FP. Cooperativity in oxidations catalyzed by cytochrome P450 3A4. Biochemistry. 1997; 36:370–381. [PubMed: 9003190]
34. Domanski TL, He YA, Harlow GR, Halpert JR. Dual role of human cytochrome P450 3A4 residue Phe-304 in substrate specificity and cooperativity. J Pharmacol Exp Ther. 2000; 293:585–591. [PubMed: 10773032]
35. Hanson KL, VandenBrink BM, Babu KN, Allen KE, Nelson WL, Kunze KL. Sequential metabolism of secondary alkyl amines to metabolic-intermediate complexes: opposing roles for the secondary hydroxylamine and primary amine metabolites of desipramine, (s)-fluoxetine, and N-desmethyldiltiazem. Drug Metab Dispos. 2010; 38:963–972. [PubMed: 20200233]
36. Lutz JD, Fujioka Y, Isoherranen N. Rationalization and prediction of in vivo metabolite exposures: the role of metabolite kinetics, clearance predictions and in vitro parameters. Expert Opin Drug Metab Toxicol. 2010; 6:1095–1109. [PubMed: 20557268]

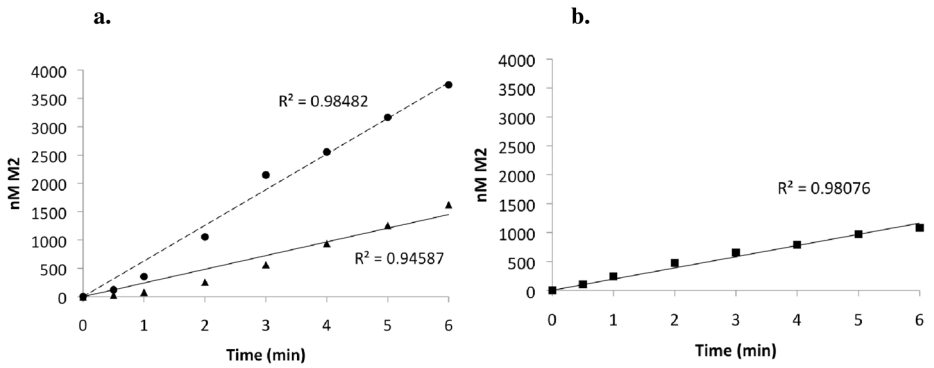

Figure 1.

Incubations of NR (a) and M1 (b) were quenched at successive time points. M2 formation from NR (triangles) shows signs of a lag in formation rate, indicative of the sequential steps required for M2 production from NR. When incubating M1 with CYP3A4 no lag in M2 formation is evident (squares). When 12 μM ANF is included in the NR incubation (circles, dotted line) the lag is seen to decrease as judged by the R^2 value and the amount of M2 produced is increased more than two-fold at six minutes.

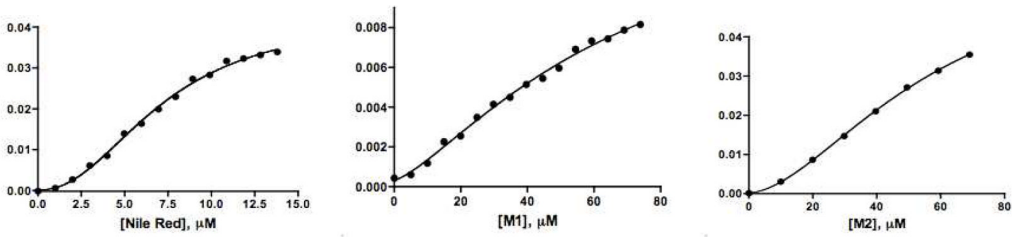

Figure 2.

Plots of spin-state perturbation vs. ligand concentration of NR and metabolites all yield sigmoidal binding titrations. Recovered S_{50}'s from fits to the Hill equation are 7.3, 68, and 58 μM for NR, M1, and M2 respectively.

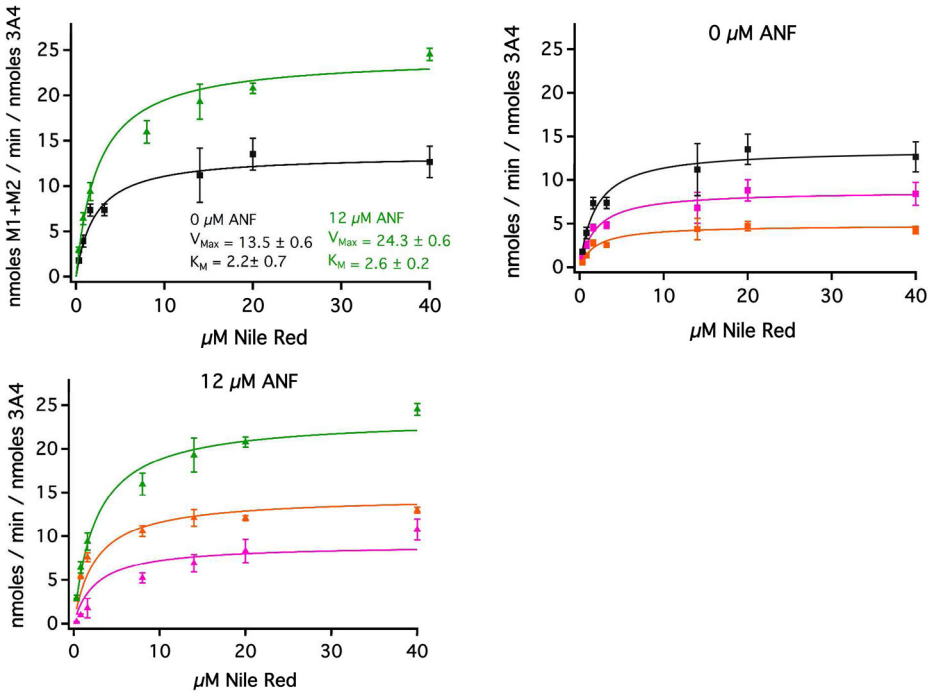

Figure 3.

Steady-state metabolism of Nile Red. The first panel shows total metabolite production (M1 + M2) for 0 μM ANF (black) and 12 μM ANF (green). The fit is to the M-M equation and illustrates that the ANF effect is on V_{Max} while K_M is not significantly different. The K_M values were used to parameterize the global fits. The second and third panels show M1 (pink), M2 (orange), and total metabolite (black or green) formation rates are plotted vs. NR concentration. The three data sets in each panel are fitted globally to the Steady-State velocity equations as detailed in Materials and Methods. The ANF stimulatory effect on M2 production is larger than the effect on M1, indicating the possible role of branch point modulation. See Table 2 for extracted rate constants.

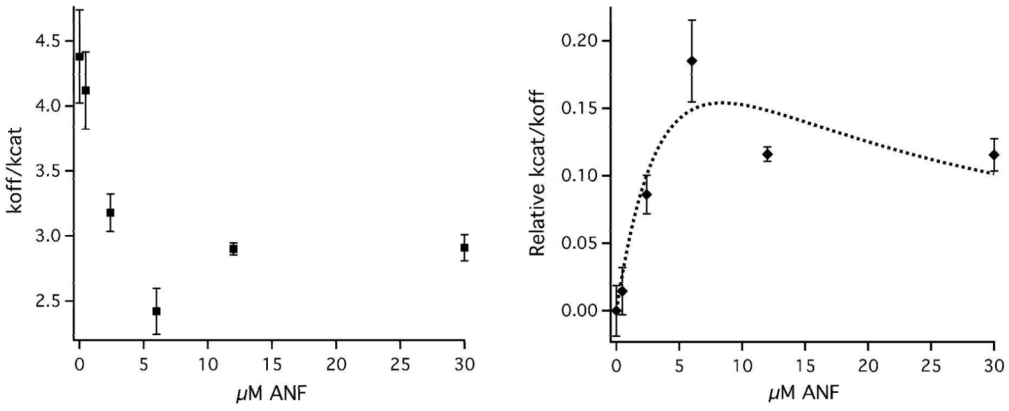

Figure 4.

The branching ratio (left) and inverse branching ratio (right; for ease of fitting, the lowest ratio was by set at zero) of NR sequential metabolism as determined by Isotope Dilution are plotted. ANF has the effect of increasing the sequential vs. dissociative M2 production. The inverse branching ratio (right) is fit to a sequential-binding substrate inhibition equation to give two affinity constants.

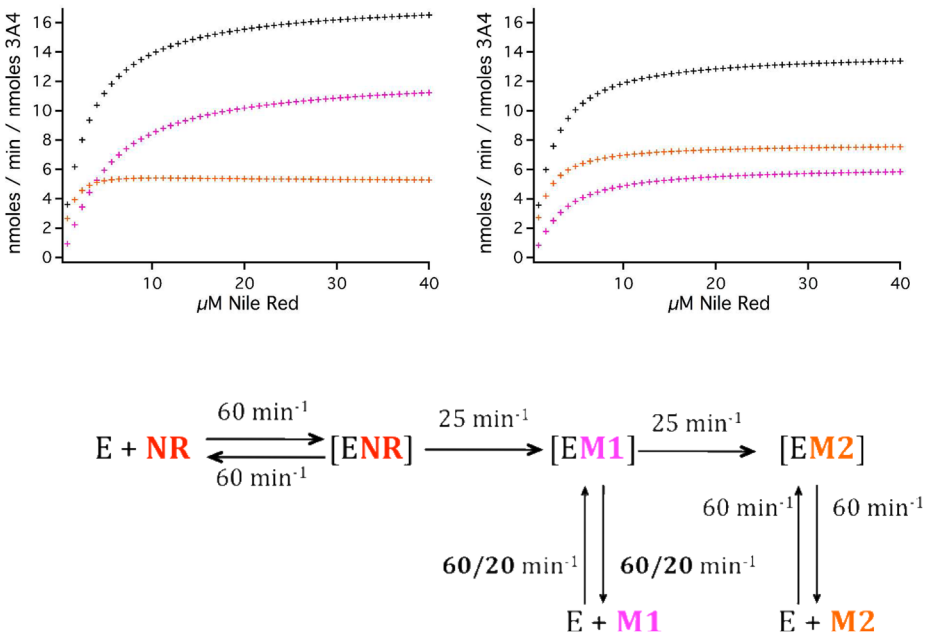

Figure 5.

Simulated NR metabolism. M1 formation is represented in pink, M2 formation in orange, and total metabolite in black. The kinetic constants (min^{-1}) for the simulation on the left are in reference to Scheme 2 and are k_1=60 k_{-1}=60 k_2=25 **k_3=60 k_{-3}=60** k_4=25 k_5=60 and k_{-5}=60. Bimolecular rate constants have units of $\mu M^{-1}min^{-1}$. Values for the graph on the right are k_1=60 k_{-1}=60 k_2=25 **k_3=20 k_{-3}=20** k_4=25 k_5=60 and k_{-5}=60. The values that change are in bold for emphasis. Importantly, this simulation shows that the M1/M2 metabolite ratio can change by modulating only the off-rate of M1, and even if the M1 K_D does not change. In this scenario, however, the total metabolite production does not increase, and so we conclude that ANF must be modulating catalysis rates in addition to M1 dissociation rates.

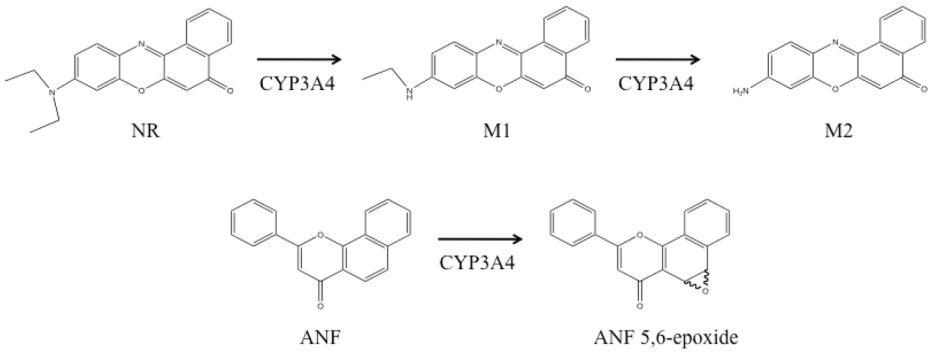

Scheme 1.

NR and ANF metabolites. NR is sequentially N-deethylated to its mono-ethyl and di-desethyl metabolites. ANF is metabolized to the 5,6-oxide.

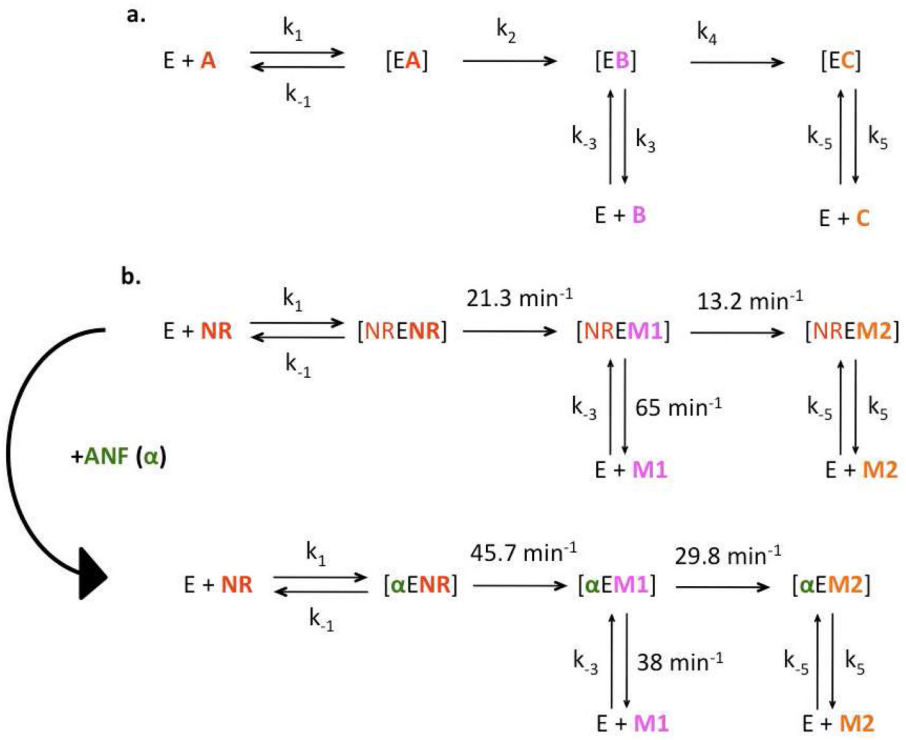

Scheme 2.

(**a**) Below is an illustration of the general case of sequential metabolism of substrate A to two products, primary metabolite B and secondary metabolite C. For the specific case of NR metabolism, NR = A, M1 = B, and M2 = C. The scheme assumes irreversible chemical steps and reversible binding. Equations for global analysis of NR metabolism were derived using the steady-state approximation according to the King-Altman method (26). Because of the sequential nature of NR metabolism, the concentration of the [EB] species is not in rapid equilibrium; it thus depends on the catalysis rates k_2 and k_4, in addition to the dissociation rate constant for B, $K_{d,B} = (k_{-3}/k_3)$. (**b**) Estimated rate constants for NR sequential metabolism with and without ANF. Catalytic rate constants are not microscopic rate constants because they include each of the rates in the P450 cycle, and so represent a flux through a pathway with multiple branching points rather than a rate constant.

Table 1

Retention times and mass transitions for metabolite identification and quantification.

Compound	Retention Time (min)	Mass Transition (m/z)
Nile Red	7.43	319->275
d_2-Nile Red	7.43	321->277
M1	5.21	291->247
d_2-M1	5.19	293->249
M2	2.81	263->190
d_2-M2	2.78	265->192
ANF	5.63	273->115
ANF-oxide	3.54	289->131
Carbamazepine	1.54	237->193

Table 2

Measured and calculated kinetic constants for NR sequential metabolism from Figure 3. The first two columns are the V_{Max} values for M1 and M2 formation fit to the M-M equation and represent nominal rates of formation irrespective of enzyme species distribution. The third column is the $V_{Max,C}$ from the B–H global analysis and represents an estimate for k_4 in both the NR homotropic species (0 μM ANF) and the heterotropic (12 μM ANF). The next two columns are ratios that estimate the fraction of enzyme metabolizing NR and enzyme metabolizing M1. The k_3 (k_{off}-M1) can then be calculated, and a theoretical branching ratio k_{off}/k_{cat}, using $V_{Max,C}$ as k_4.

	(A–>B) M1 Rate *min*$^{-1}$	(A–>C) M2 Rate *min*$^{-1}$	"(B–>C)" $V_{Max\ C}$ *min*$^{-1}$	(A–>C)/(A–>B) M2 Rate / M1 Rate	(A–>C)/"(B–>C)" [EB]/([EA]+[EB]) *Fraction [EB]*	Koff-M1 *min*$^{-1}$	Koff/Kcat	$V_{Max\ B}$ *min*$^{-1}$
0 μM ANF	8.9±0.4	4.9±0.2	13.2±3.2	0.55	0.37	65	4.89	21.3±2.2
12 μM ANF	8.9±0.8	14.4±0.8	29.8±6.6	1.62	0.48	38	1.28	45.7±6.9